AIAA JOURNAL
Vol. 47, No. 9, September 2009

Investigation of Rotor Wake Turbulence Through Cyclostationary Spectral Analysis

Vincent Jurdic* and Phillip Joseph†
University of Southampton, Southampton, England SO17 1BJ, United Kingdom
and
Jerome Antoni‡
University of Technology of Compiegne, 60205 Compiegne Cedex, France

DOI: 10.2514/1.36728

The present paper introduces cyclostationary spectral analysis as a new approach to analyze the turbulence velocity measurements generated by a rotor. To apply this technique, a random signal should have periodic statistical characteristics and should be suitable for many rotating mechanical system as shown in recent studies. However, this method has never been applied on rotor velocity measurements. Via a Wigner–Ville representation, the instantaneous power spectra of the turbulence in the wakes and in between the wakes will be depicted and analyzed. The usefulness of the technique applied to rotor-generated turbulence is that it can separate the spectrum of the turbulence in between the wakes from that in the wake with a much greater frequency resolution than conventional spectral analysis.

Nomenclature

F_s	=	sampling frequency, Hz
f	=	frequency, Hz
K	=	number of cycle in the measurements time length
L	=	number of samples of the measurement
L_w	=	wake width, m
m_{w}	=	coherent velocity average, m/s
N	=	number of samples per cycle
N_s	=	number of overlapping samples between adjacent segments
N_v	=	window length
$\mathcal{R}_{ww}$	=	instantaneous autocorrelation function, m^2/s^2
$\mathcal{R}_{ww,\alpha_j}$	=	cyclic autocorrelation function, m^2/s^2
r	=	radius, m
$\mathcal{SC}_{ww}$	=	spectral correlation, m^2/s^2 Hz^2
$\mathcal{S}_{ww,\alpha_j}$	=	cyclic power spectrum, m^2/s^2 Hz
T	=	cycle time, s
T_{BPF}	=	time duration between two successive blades passage, s
t	=	time, s
v	=	window
$\mathcal{WV}_{ww}$	=	Wigner–Ville spectrum
$\bar{\mathsf{w}}$	=	mean value, m/s
$\mathsf{w}(t)$	=	total measured velocity, m/s
$w(t)$	=	fluctuating velocity component, m/s
$\overline{w^2}(t)$	=	instantaneous variance, m^2/s^2
α_j	=	cyclic frequency, Hz
Λ	=	turbulence length scale, m
θ	=	circumferential position, deg
τ	=	time lag, s
φ	=	lag angle, deg
Ω	=	rotation speed, rad/s

Subscripts

exp	=	measurement
rot	=	shaft rotation

Superscript

$*$	=	conjugate of

I. Introduction

THE trend toward higher bypass ratio engines and more effective duct liners has yielded significant reductions in jet noise and fan tone noise. By contrast, fan broadband noise has been hardly affected by these advances and contribute largely to the noise pollution of a modern aircraft engine. It has long been recognized that fan broadband noise is mainly generated by the interaction between the turbulent rotor wakes and the stator vanes and also rotor self-noise, due to the interaction between the rotor blade boundary layer and its trailing edge. Recent work by Nallasamy and Envia [1], however, has suggested that the turbulence in between the wakes, that is, the background turbulence, could be as important as that in the wakes themselves for producing broadband noise. This suggestion is supported by the recent work of Jurdic et al. [2]. Both Nallasamy and Envia [1] and Jurdic et al. [2] have quantified the broadband noise due to turbulence in between the wakes compared with that in the wakes. They found that the former generates broadband levels that are just a few decibels below that due to wake turbulence and cannot therefore be neglected. The turbulence in between the wakes most likely originates from turbulence in the atmosphere being ingested into the engine. This background turbulence is therefore totally unrelated to the wake turbulence and has completely different statistical characteristics. An accurate noise model must therefore include the detailed characteristics of each source of turbulence separately. In the work of Nallasamy and Envia [1] and Jurdic et al. [2], however, it was necessary to assume a spectral form, length scales, and levels for these turbulence sources separately, as no direct measurements of these sources individually have hitherto been possible.

Experimental studies undertaken by Ganz et al. [3] and Gliebe et al. [4] have measured the spectra of rotor-generated velocity fluctuation downstream of a rotor in attempt to extract the turbulence characteristics. However, the spectra were estimated assuming statistically stationarity of the velocity signals. However, for the aforementioned reasons, the rotor-generated velocity signals are clearly not stationary. The turbulence spectra obtained by these

Received 28 January 2008; revision received 8 October 2008; accepted for publication 19 March 2009.

*Institute of Sound and Vibration Research, University Road, Highfield; vj@isvr.soton.ac.uk.
†Institute of Sound and Vibration Research, University Road, Highfield; pfj@isvr.soton.ac.uk.
‡Laboratory Roberval of Mechanics.

authors using classical stationary spectral analysis are therefore ambiguous, particularly as they also include both background and wake turbulence spectra, which are significantly different, as demonstrated in Sec. IV.

As discussed previously, classical stationary spectral analysis applied to short-time duration windows is not practicable as a way of separating the turbulence spectrum in between the wakes from that in the wakes. A typical instantaneous velocity measurement is shown in Fig. 1. It corresponds to the velocity component normal to the stator chord, measured in a scale fan rig at DLR in Berlin, at a midspan position 11.5-mm downstream of the rotor. With reference to Fig. 1, the time duration t_w of the wakes generated by the rotor blades and the time duration t_b between successive wake arrivals are too short to allow spectral estimates with sufficient frequency resolution. Since $t_w + t_b = T_{\mathrm{BPF}}$, where T_{BPF} is the time duration between two successive blades passage, their corresponding frequency resolutions $\Delta f_w = 1/t_w$ and $\Delta f_b = 1/t_b$ will therefore be greater than the blade passing frequency (BPF), that is, Δf_w, $\Delta f_b > \mathrm{BPF} = 1/T_{\mathrm{BPF}}$, where BPF is generally greater than 1 kHz.

This paper describes a new approach to the analysis of the unsteady velocity measurements generated by a fan that allows the wake and background turbulence characteristics to be separated. This technique allows the spectra to be determined with a much higher frequency resolution than that obtained using classical spectral analysis. The analysis method exploits the property that the signal statistics are cyclostationary. A cyclostationary signal is a random signal whose statistical characteristics vary periodically in time. Cyclostationary theory was developed initially for telecommunications applications in which the data are modulated by a carrying sinusoidal signal. Cyclostationary spectral analysis has also been applied to many mechanical systems involving rotating elements by Antoni et al. [5] and Bonnardot et al. [6]. However, little work has been undertaken on the use of this method in aerodynamic application to characterize unsteady time periodic turbulent flows [7] and aeroacoustic application to analyze typical helicopter noise signals [8]. An extensive review of the cyclostationarity theory and its applications has been presented by Gardner et al. [9].

Section II of this paper presents the outline of cyclostationary theory. The first- and second-order moments will be defined. It will be shown that classical stationary analysis can be considered as a special case of cyclostationary analysis. Section III reviews the details of the DLR rig in Berlin on which the experimental data analyzed in this paper were made. Section IV describes the application of cyclostationary analysis to the interstage velocity measurements to separate the wake and background turbulence characteristics.

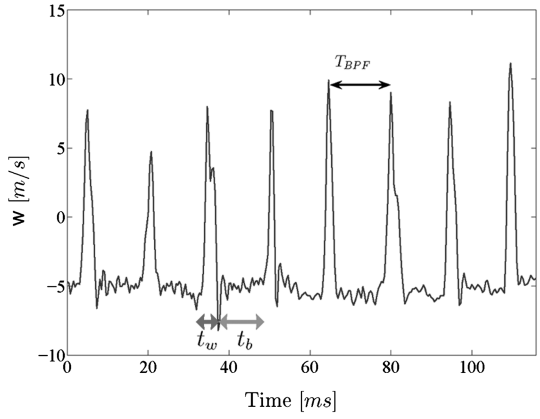

Fig. 1 Example of the DLR fan rig velocity measurements behind a rotor, t_b background time duration, t_w wake time duration, and T_{BPF} blade passing time duration.

II. Cyclostationary Theory

Any random signal whose statistical characteristics are periodic is classified as a cyclostationary signal. The definition includes deterministic periodic signals. To avoid confusion with this type of signal, the period of the statistical characteristics is called the cycle. Stationary processes correspond to the special case of a cyclostationary process in which the cycle time tends to infinity. The classical statistical estimators for stationary signals can be extended to cyclostationary signals. These are discussed next.

A. Cycloergodicity

The ensemble average $\mathbb{E}\{\,\}$ of a random signal involves repeated experiments with the results averaged together. By assuming that the signal is ergodic, which implies the signal is also stationary, the ensemble-average operator $\mathbb{E}\{\,\}$ can be replaced by the time-average operator:

$$\mathbb{E}\{\mathsf{w}\} = \lim_{T_{\exp}\to\infty} \frac{1}{T_{\exp}} \int_0^{T_{\exp}} \mathsf{w}(t)\,\mathrm{d}t \tag{1}$$

The ergodicity assumption significantly simplifies experimental design because the statistical characteristics can be estimated from an experiment of sufficiently long duration.

For a cyclostationary process, the ergodicity assumption is inappropriate because the time average and ensemble average will give different results. However, Boyles and Gardner [10] have extended the ergodicity principle to define the notion of cycloergodicity for a cyclostationary process. The ensemble average is therefore replaced by a cycle average. Each measurement segment is averaged with each other one cycle apart. Braun [11] has introduced the following cycle averaging operator, or time domain averaging, to estimate the ensemble-average operator $\mathbb{E}\{\,\}$:

$$\mathbb{E}\{\mathsf{w}(t)\} = \lim_{K\to\infty} \frac{1}{K} \sum_{k=0}^{K} \mathsf{w}(t + kT) \tag{2}$$

Because Eq. (2) corresponds to an operator with periodicity of T, it can be expressed as a Poisson sum by

$$\mathbb{E}\{\mathsf{w}(t)\} = \sum_{k=-\infty}^{\infty} e^{i2\pi kt/T} \left\{ \lim_{s\to\infty} \frac{1}{s} \int_{-s/2}^{s/2} \mathsf{w}(u) e^{-i2\pi ku/T}\,\mathrm{d}u \right\} \tag{3}$$

where the term in curly brackets is the Fourier transform of $\mathsf{w}(t)$.

These two definitions of the cycle operator are equivalent. Equation (2) is efficient but can only be used when the cycle time T, sampled at the frequency F_s, is equal to an integer number N of samples per cycle, such that $T = N/F_s$. In other cases, Eq. (3) is more appropriate.

Just as the ergodicity assumption requires a long measurement time, the cycloergodicity assumption also implies the availability of measurements corresponding to a large number K of cycles.

The ergodicity and cycloergodicity concept has been often criticized for its probabilistic relationship. Gardner [12] has proposed the fraction-of-time probability concept, more appropriate to analyzing experimental data. However, this approach implies relatively complicated considerations. To keep the article accessible to readers unfamiliar with the theory of stochastic processes, the authors have chosen to refer to the ergodicity concept, which was introduced and accepted a long time ago.

In the following sections, reference to a stationary process implies that the turbulence velocity signal is ergodic [the ensemble averaging is replaced by Eq. (1)], whereas referring to a cyclostationary process implies that the signal is cycloergodic [the ensemble averaging is replaced by Eq. (2) or Eq. (3)].

B. First-Order Moments: The Coherent Average

The first-order moment of any signal $\mathsf{w}(t)$ is obtained by averaging the signal over different repeated experiments:

$$m_{\mathsf{w}}(t) = \mathbb{E}\{\mathsf{w}(t)\} \tag{4}$$

For a stationary process, the first-order moment is independent of time and defines the mean value $\bar{\mathsf{w}}$ by

$$m_{\mathsf{w}} = \bar{\mathsf{w}} = \lim_{T\to\infty} \frac{1}{T}\int_0^T \mathsf{w}(t)\,\mathrm{d}t \tag{5}$$

For a cyclostationary process, the first-order moment is periodic and defines the coherent average, also called the time domain average [11] or synchronous average [5]:

$$m_{\mathsf{w}}(t + kT) = m_{\mathsf{w}}(t) \tag{6}$$

where k is any integer.

Note that the coherent average is identical to the technique proposed by Evans [13]. The coherent average describes the evolution of the mean signal during a cycle. For measurements of the velocity generated by a rotor, the coherent average will therefore estimate the mean wake profile during one rotation, assuming that the cycle is taken to be the time taken for one shaft rotation.

The measured velocity signal $\mathsf{w}(t)$ can be decomposed as the sum of the coherent average $m_{\mathsf{w}}(t)$ plus a fluctuating random component corresponding to the turbulent velocity fluctuations $w(t)$:

$$\mathsf{w}\,(t) = m_{\mathsf{w}}(t) + w(t) \tag{7}$$

C. Second-Order Moments

The various second-order moments of a cyclostationary signal characterize its power distribution. The definitions of the second-order moments are now presented for the fluctuating velocity component $w(t)$, obtained from Eq. (7). Note that these are identical to the second-order cumulant of the total velocity $\mathsf{w}(t)$, suggested by Antoni et al. [5].

1. *Autocorrelation Function*

The autocorrelation function quantifies the dependence of a signal at a moment in time to the signal at a short time later (or before). One definition of the autocorrelation function of $w(t)$ at a time t is

$$\mathcal{R}_{ww}(t,\tau) = \mathbb{E}\{w(t+\tfrac{1}{2}\tau)w^*(t-\tfrac{1}{2}\tau)\} \tag{8}$$

Whereas the autocorrelation function is independent of time t for stationary signals, for a cyclostationary signal, it has the periodicity property

$$\mathcal{R}_{ww}(t + kT, \tau) = \mathcal{R}_{ww}(t,\tau) \tag{9}$$

Verification that this property is closely observed for rotor-generated wake velocity data is presented in Sec. IV.

2. *Cyclic Autocorrelation Function*

The periodic autocorrelation function of Eq. (9) can be expressed as the Fourier series expansion

$$\mathcal{R}_{ww}(t,\tau) = \sum_{\alpha_j} \mathcal{R}_{ww,\alpha_j}(\tau) e^{i2\pi\alpha_j t} \tag{10}$$

where $\alpha_j = j/T$, j being an integer.

The Fourier coefficients $\mathcal{R}_{ww,\alpha_j}$ of Eq. (10) are only a function of τ and are called the cyclic autocorrelation or cyclocorrelation function. They are obtained by inverting Eq. (10) to give

$$\mathcal{R}_{ww,\alpha_j}(\tau) = \frac{1}{T}\int_{-T/2}^{T/2} \mathcal{R}_{ww}(t,\tau) e^{-i2\pi\alpha_j t}\,\mathrm{d}t \tag{11}$$

Note that, for $\alpha_j = 0$, the cyclic autocorrelation function corresponds to that with assumed stationarity, that is, the autocorrelation, averaged over t.

Equation (10) forms the basis of the method proposed here for separating from the measured data the wake turbulence and the background turbulence. We assume that the background turbulence is a purely stationary process with no periodic components, that is, $\alpha_j = 0$. By contrast, wake turbulence is assumed to contain all periodic components α_j, including $\alpha_j = 0$. The method for separating the background and wake turbulence components associated with $\alpha_j = 0$ will be made clear in Sec. IV.

3. *Spectral Correlation*

Measurements of the turbulence velocity fluctuations are often presented in the frequency domain to describe the spectral content of the signal. For a stationary signal, the Fourier transform over τ of the autocorrelation function of Eq. (8) yields the power frequency spectrum. In the case of a cyclostationary process, the autocorrelation function depends on the time t and the time lag τ. The Fourier transform over these two parameters t and τ defines the spectral correlation function $\mathcal{SC}_{ww}$:

$$\mathcal{SC}_{ww}(\alpha, f) = \int_{-\infty}^{\infty}\int_{-\infty}^{\infty} \mathcal{R}_{ww}(t,\tau) e^{-i2\pi\alpha t} e^{-i2\pi f\tau}\,\mathrm{d}t\,\mathrm{d}\tau \tag{12}$$

which characterizes the power distribution versus spectral frequency f for each discrete cyclic frequency component α. The variation with α quantifies the frequency content of the energy distribution of the nonstationary signal $w(t)$ during the cycle T.

It can be shown in more specialized articles about cyclostationary spectral analysis, reviewed by Gardner et al. [9], that $\mathcal{SC}_{ww}$ can also be expressed as

$$\mathcal{SC}_{ww}(\alpha, f) = \lim_{T\to\infty} \frac{1}{T}\mathbb{E}\left\{W_T\left(f + \frac{1}{2}\alpha\right) W_T^*\left(f - \frac{1}{2}\alpha\right)\right\} \tag{13}$$

where $W_T(f)$ is the short-time Fourier transform of $w(t)$ over large but finite duration T:

$$W_T(f) = \int_{-T}^{T} w(t) e^{-i2\pi f t}\,\mathrm{d}t \tag{14}$$

Equation (13) indicates that $\mathcal{SC}_{ww}(\alpha, f)$ quantifies the correlation between two spectral components of a single signal separated in frequency by α.

4. *Cyclic Power Spectrum*

Substituting Eq. (10) into Eq. (12) reveals that the spectral correlation is discrete in α frequency and continuous in the spectral frequency f, and can therefore be written in the form

$$\mathcal{SC}_{ww}(\alpha, f) = \sum_{\alpha_j} \mathcal{S}_{ww,\alpha_j}(f)\delta(\alpha - \alpha_j) \tag{15}$$

where δ is the Dirac delta function. Here, we assume that, because the background turbulence is nonperiodic, it therefore only contributes to the term $\mathcal{S}_{ww,0}$.

The cyclic power spectrum can be interpreted as a generalization of the power spectrum $\mathcal{S}_{ww}(f)$ for stationary signals, that is, $\mathcal{S}_{ww,0}(f) = \mathcal{S}_{ww}(f)$. The cyclic power spectrum can also be defined in terms of the Fourier transform of the cyclic autocorrelation function $\mathcal{R}_{ww,\alpha_j}(\tau)$:

$$\mathcal{S}_{ww,\alpha_j}(f) = \int_{-\infty}^{\infty} \mathcal{R}_{ww,\alpha_j}(\tau) e^{-i2\pi f\tau}\,\mathrm{d}\tau \tag{16}$$

5. *Wigner–Ville Spectrum*

For finite energy deterministic signals, the Wigner–Ville distribution has been introduced to quantify the time evolution of the frequency power spectrum [14]. In the case of a stochastic process, the Wigner–Ville spectrum $\mathcal{WV}_{ww}(t, f)$ is used to quantify the instantaneous power spectrum of the signal at time t. It can be obtained either from the autocorrelation function $\mathcal{R}_{ww}$ by

$$\mathcal{WV}_{ww}(t,f) = \int_{-\infty}^{\infty} \mathcal{R}_{ww}(t,\tau) e^{-i2\pi f\tau}\,\mathrm{d}\tau \tag{17}$$

or from the cyclic power spectrum $\mathcal{S}_{ww,\alpha_j}$ by

$$\mathcal{WV}_{ww}(t,f) = \sum_{j=-\infty}^{\infty} \mathcal{S}_{ww,\alpha_j}(f) e^{i2\pi\alpha_j t} \tag{18}$$

Because the blade position can be known precisely at any instant in time, the Wigner–Ville spectrum allows the turbulence velocity spectra in between the wakes (background turbulence) and in the wake (wake and background turbulence).

6. *Summary of the Second-Order Moments*

The interrelationship between the various quantities previously discussed for the various classes of process is shown in Fig. 2. The cyclostationary class is a specific case of the nonstationary class, as the nonstationarity is limited to the cycle duration T and is then repeated indefinitely. When the cycle duration tends to zero, the process tends to stationarity.

Section IV will show that the background turbulence can be identified as a stationary nonperiodic process, whereas the wake turbulence corresponds to a cyclostationary process.

7. *Instantaneous Variance*

For stationary signals, its variance quantifies the energy of the signal and, for zero-mean signals, is defined as the mean square value of $w(t)$:

$$\overline{w^2} = \mathbb{E}\{w^2(t)\} = \mathcal{R}_{ww}(0) = \int_{-\infty}^{\infty} \mathcal{S}_{ww}(f)\,\mathrm{d}f \tag{19}$$

In the case of a cyclostationary signal $w(t)$, the instantaneous variance can be similarly defined to describe the variation of the mean square turbulence velocity over the cycle:

$$\overline{w^2}(t) = \mathcal{R}_{ww}(t,0) = \int_{-\infty}^{\infty} \mathcal{WV}_{ww}(t,f)\,\mathrm{d}f \tag{20}$$

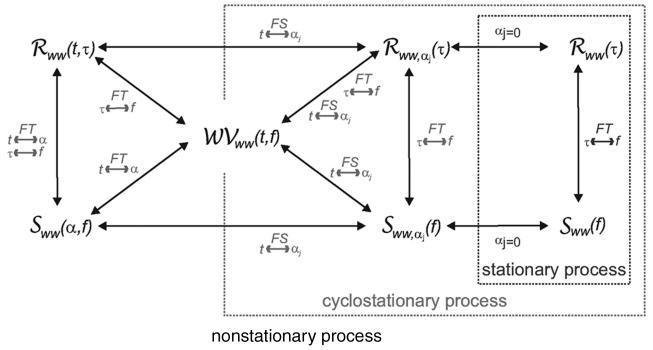

Fig. 2 Diagram showing the relations between the various second-order moments for different classes of process.

In the present application, $\overline{w^2}(t)$ corresponds to the turbulence intensity profile through the wake. From Eqs. (9) and (20), $\overline{w^2}(t) = \overline{w^2}(t + kT)$.

Finally, the cyclic-spectral distribution of the instantaneous variance $\overline{w^2_{\alpha_j}}$ can be calculated from

$$\overline{w^2_{\alpha_j}} = \int_{-\infty}^{\infty} \mathcal{SC}_{ww}(\alpha_j, f)\,\mathrm{d}f \tag{21}$$

which quantifies the mean square velocity contribution from each cyclic frequency component α_j. The discrete time Fourier transform of the instantaneous variance is therefore a discrete function of α_j and characterizes the energy distribution over the cycle. Recall that $\overline{w^2_0}$ is the sum of contributions from the background turbulence and from the wake turbulence for $\alpha = 0$.

III. Experimental Setup

In this section, we describe the experimental rig on which the rotor velocity data were obtained as part of the European project PROBAND. Velocity measurements were made at two axial positions in between the rotor and stator in a low-speed fan rig (Fig. 3) at DLR. The fan stage consists of a 24-bladed rotor and a 16-vaned stator. A tacho signal has been used to locate the blade positions, and the velocity measurements resampled such that there are 39 measurements points between adjacent blades. Each shaft rotation is then composed of 936 data points. More details on the experimental setup can be found in previous papers by Moreau et al. [15] and Jurdic et al. [2].

Turbulence measurements were also made of the flow entering the duct inlet. A cross hot-wire probe was used to measure the radial and axial turbulence velocities in the duct section upstream of the rotor fan. The mean velocity was found to be relatively constant along the radius and was equal to 17 m/s. The turbulence intensity has been found to increase from 2% in the midduct to 3.5% at the upper wall. The axial and radial turbulence length scales were estimated by integrating the temporal autocorrelation function over time. The axial turbulence length scale is found to increase from 30 mm in the midduct to 60 mm at the upper wall, whereas the radial length scale tends to decrease from 40 to 5 mm.

IV. Cyclostationary Analysis

By way of example, cyclostationary spectral analysis will be applied to the velocity measurements made at a position 11.5-mm downstream of the rotor trailing edge at the midspan position along the stator vanes. At this location, secondary flows generated by the hub or the tip walls are negligible. This paper will focus on the component of the turbulence velocity normal to the leading edge of the stator vanes, corresponding to the upwash velocity at the stator vanes. This is the component known to be important for noise generation [16]. The quantities $\mathsf{w}(t)$, $m_{\mathsf{w}}(t)$, and $w(t)$ therefore correspond to the total velocity, the coherent velocity, and the fluctuating velocity components normal to the stator chord, respectively.

Cyclostationary analysis requires the cycle time T to be known a priori. The obvious choice is the time taken to complete one shaft rotation. Another equally reasonable choice of T, based on the

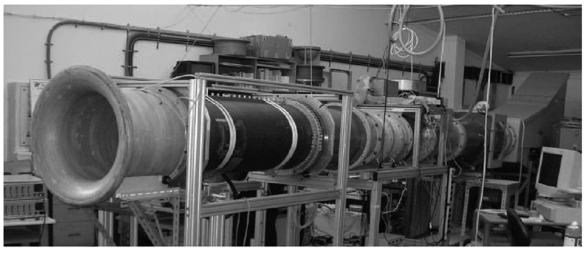

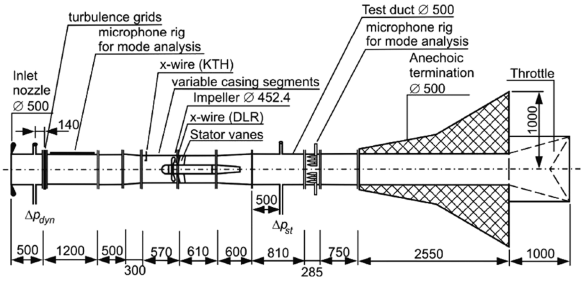

Fig. 3 Photograph (left) and schematic overview (right) of the DLR-Berlin fan rig with instrumentation (KTH: Kungliga Tekniska högskolan).

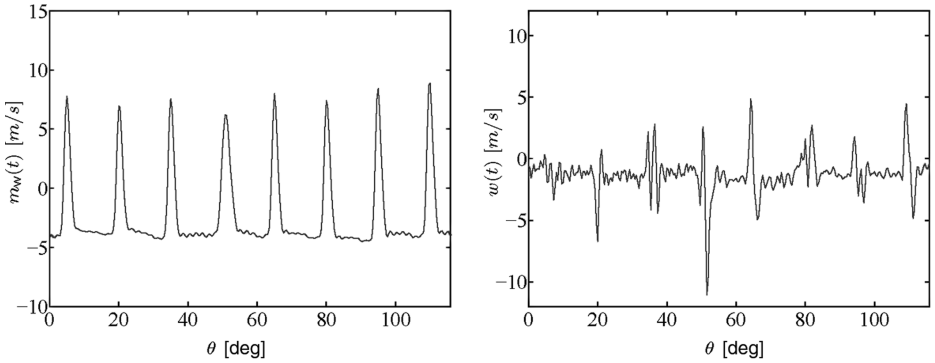

a) Coherent velocity component $m_w(t)$ **b) Fluctuating velocity component $w(t)$**

Fig. 4 Measured mean and fluctuating velocity components.

assumption that the blade wakes are statistically identical, is the time taken between successive blade arrivals T_{BPF}.

The resampling of the velocity measurements, linked to the shaft rotation speed, means that each cycle is composed of a finite number of samples $N = 936$. The obvious cycle duration corresponds to the time for one blade to complete one full rotation, such that $T_{\text{rot}} = N/F_s = 936/F_s$. The cyclostationary analysis results presented in this paper are based on a signal length corresponding to $K = 200$ cycles.

A. Coherent and Fluctuating Velocity Components

Figure 1 shows the time history of the total measured velocity component $\mathsf{w}(t)$ normal to the stator chord. Because the number of samples per cycle N is an integer, Eq. (2) can be used to estimate the coherent average and is presented in Fig. 4a. The coherent average, presented in this paper, corresponds to the mean upwash velocity wake profiles that are responsible for generating tones at BPF and its harmonics. Because the upwash velocity is only one component of the velocity vector and not the velocity magnitude, its value is negative in between the wakes. Figure 4b presents the fluctuating velocity component $w(t)$, obtained from Eq. (7).

Each mean wake in Fig. 4a is slightly different from the other, suggesting that all blades are not exactly identical. These differences appear in the acoustic spectrum as tones at harmonics of the shaft rotation frequency (not shown in this paper). However, these tones are not easily observed and most of the tones occur at harmonics of the BPF.

The fluctuating part of the velocity signal, plotted in Fig. 4b, shows significant levels of unsteady velocity in between the wakes and generally higher levels in the wakes themselves.

Because the shaft rotation speed Ω can be considered as constant for the present case, the time t and lag τ parameters have therefore been replaced in the following figures by the circumferential position $\theta = \Omega t$ of the wake in relation to the measurement point and the correlation lag angle $\varphi = \Omega\tau$, respectively.

B. Instantaneous Variance and Its Cyclic-Spectral Distribution

The instantaneous variance $\overline{w^2}(t)$ can be obtained from Eq. (19). It corresponds to the coherent average of $w^2(t)$ and relates directly to the turbulence mean square velocity through the wakes. It is plotted versus circumferential blade position θ in Fig. 5.

The instantaneous variance between the wakes ($\overline{w_b^2} \approx 1.35\ \text{m}^2/\text{s}^2$) is clearly significant compared to that in the wakes themselves ($10 < \overline{w_w^2} < 20\ \text{m}^2/\text{s}^2$), particularly as $t_b > t_w$ in this case. The classical "double hump" behavior due to the presence of shear layers is clearly seen. The largest hump occurs at blade pitch angles corresponding to the shear layer in the blade pressure side, whereas the smallest hump is due to the shear layer generated by the blade suction side. The turbulence energy in the wakes exhibits significant variations from blade to blade suggesting the presence of harmonics at multiples of the shaft rotation frequency.

The mean square velocity distribution $\overline{w_{\alpha_j}^2}$ of the instantaneous variance $\overline{w^2(t)}$ for each cyclic order α_j defined by Eq. (21) is plotted in Fig. 6 versus the cyclic frequency nondimensionalized by the shaft rotation time T_{rot}. Such a normalization defines a cyclic engine order (CEO), defined by $\text{CEO} = \alpha_j/T_{\text{rot}}$. Also shown as the dashed curve is a Gaussian curve, which can be seen to provide a close fit to the $\overline{w_{\alpha_j}^2}$ distribution, except, as expected, for $\alpha_j = 0$, where there are contributions from the background turbulence.

Most of the turbulence energy is seen to be concentrated at harmonics of the BPF, $\text{CEO}_j = jB$, although significant components occur at other CEOs corresponding to blade-to-blade differences in the wake statistical characteristics. This result suggests, therefore, that the basic cycle of the process is the time taken between two adjacent blades $T_{\text{BPF}} = T_{\text{rot}}/B$, indicating that the turbulent wakes from each blade are statistically similar. In view of the preceding discussion, the results of the spectral analysis, presented next, are obtained by assuming a cycle duration of $T = T_{\text{BPF}} = 39/F_s$ over a number of cycles $K = 200B$. However, the cyclostationary spectral

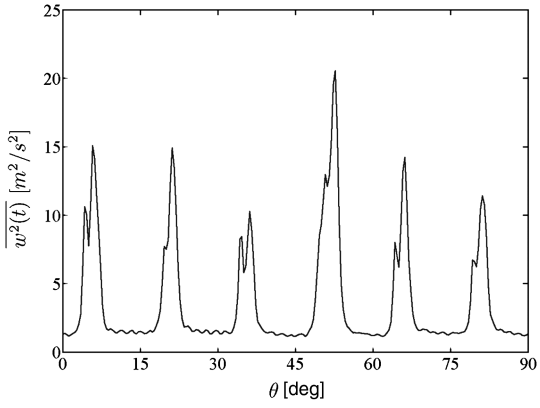

Fig. 5 Instantaneous variance of the measured velocity $\mathsf{w}(t)$ with the cycle $T = T_{\text{rot}}$.

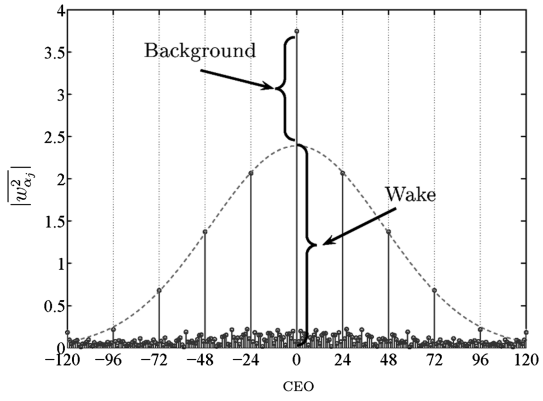

Fig. 6 Cyclic-spectral distribution of the instantaneous variance of the measured velocity $\mathsf{w}(t)$ (solid line) and Gaussian fitting (dashed line).

analysis is also performed with the fluctuating velocity $w(t)$ obtained assuming $T = T_{\text{rot}}$ and hence individual blade wake profiles.

The classical two-dimensional plane wake theory due to Wygnanski et al. [17] has demonstrated that, for two-dimensional wakes, based on similarity arguments, the mean wake velocity profile for a two-dimensional plane wake, many momentum thicknesses downstream, closely follows a Gaussian function. Ganz et al. [3] has shown also that the rms velocity on the wake is roughly proportional to the mean wake velocity deficit. Thus, the mean square velocity variation through the wake can also be approximated to a Gaussian wake profile. This hypothesis is confirmed in Fig. 6 in which a Gaussian curve has been fitted to $|\overline{w^2_{\alpha_j}}|$ at the harmonics of BPF, that is, at CEO $= \pm 24$, CEO $= \pm 48$, CEO $= \pm 72$, and CEO $= \pm 96$ and has been plotted by a dashed line. Very close agreement is observed. As expected, the curve fit fails to fit the data at α_0 because it comprises both wake and background turbulence velocity contributions. This observation allows the separation of background and nonperiodic wake components. The background component is clearly nonnegligible compared to the nonperiodic wake component.

C. Cyclostationary Power Spectral Analysis

As discussed earlier, cyclostationary power spectral analysis allows the background and wake turbulence spectra to be separated. The various second-order moments, defined in the previous section, offer different representations of the energy of the turbulent rotor wake. Their interrelationship is shown in Fig. 2.

1. *Implementation of the Cyclic Power Spectrum*

Antoni [18] describes in detail different estimators for computing the cyclic power spectrum $\mathcal{S}_{ww,\alpha_j}$. The averaged cyclic periodogram is shown to be one of the most efficient estimators. This is the one used to analyze the measured data in this article and is described in detail next.

The averaged periodogram estimator $\mathcal{S}^L_{ww,\alpha_j}$ is based on the definition Eq. (13) of the spectral correlation. The sampled measured fluctuating velocity signal $\{w[n]\}_{n=0}^{L-1}$, is decomposed into K segments with an overlap of N_s samples between adjacent segments. Two shifted signals are generated by introducing a frequency shift of $\pm\alpha/2$ at each segment. Fast Fourier transforms (FFT) are performed on the pair of shifted signals and their product averaged over the K segments to allow the estimate of the spectral correlation. In practice, a positive and smooth window $\{v[n]\}_{n=0}^{N_v-1}$ is introduced to divide the velocity signal into K segments. The averaged cyclic periodogram is given by

$$\mathcal{S}^{\,L}_{ww,\alpha_j} = \frac{F_s}{K}\sum_{k=0}^{K-1} W^{(k)}_{N_v}\left(f+\frac{1}{2}\alpha\right) W^{(k)*}_{N_v}\left(f-\frac{1}{2}\alpha\right) \tag{22}$$

where $W^{(k)}_{N_v}(f)$ is the short-time discrete time Fourier transform (DTFT), defined by

$$W^{(k)}_{N_v}(f) = \frac{1}{F_s}\sum_{n=kR}^{kR+N_v-1} v[n-kR]w[n]e^{-i2\pi nf/F_s} \tag{23}$$

where $R = N_v - N_s$. Equation (22) is a direct consequence of Eq. (13), for which the continuous short-time Fourier transform is replaced by the DTFT.

This estimator has been presented by Antoni [18] as an extension of the stationary analysis method of Welch. This method is computationally efficient because it involves the use of the FFT. The results presented next adopt this algorithm using an FFT with 1024 data points. A Hanning window of length $N_v = 1024$ was also used, with a 67% overlap.

2. *Wake Turbulence Characteristics*

The magnitude of the spectral correlation $|\mathcal{SC}_{ww}(\alpha_j, f)|$ of the fluctuating velocity $w(t)$, defined by Eq. (16), is plotted in Fig.7 versus engine order (EO $= f/T_{\text{rot}}$) and cyclic engine order. Note that the cyclic spectrum is symmetric in α, such that $\mathcal{SC}_{ww}(-\alpha, f) = \mathcal{SC}_{ww}(\alpha, f)$. As expected, the spectral correlation has only discrete components in α, because we now assume that $T = T_{\text{BPF}}$. Through classical stationary spectral analysis (i.e., $\alpha_j = 0$) of the turbulence velocity, high amplitude peaks are observed for engine order EO $= 24, 48, \ldots$, that is, at the BPF and its harmonics. These peaks suggest that the fluctuating velocity component w still contains periodic components, even after removing the coherent part from the total measured velocity w. This is because the decomposition of the signal $\mathsf{w}(t)$ into coherent and random components as in Eq. (7) is imperfect, most likely due to small differences between various cycles. Figure 7 reveals the presence of tones at the BPF for the even cyclic frequency orders and tones at half the BPF for the odd cyclic frequency orders. These tones are not present in the acoustic spectrum, suggesting that the presence of tones at half the BPF in the velocity spectrum is an artifact of the cyclostationary spectral analysis. These spurious spectral components are a well-known occurrence of this technique and arise due to the interference between two coherent frequency components.

Assuming that the background turbulence is purely stationary in character, the cyclic power spectra for $\alpha_j \neq 0$ quantify only the spectra of the wake turbulence. In Fig. 8, the cyclic power spectra nondimensionalized by $\overline{w^2_{\alpha_j}}$ defined by Eq. (21), are plotted for different values of α. Excellent collapse of the spectra is obtained for $\alpha_j \neq 0$. Spectral shapes of each cyclic component α_j are therefore similar, suggesting that the wake turbulence has a single spectral form at all points through the wake, that is, there is no evolution of the instantaneous spectral shape through the wake.

Note that, for $\alpha_j = 0$, the turbulence power spectrum tends toward a high value as $f \to 0$ compared to that for $\alpha_j \neq 0$. However, because this low-frequency behavior appears only for the nonperiodic ($\alpha = 0$) term, it may be assumed to be a characteristic of the background turbulence. Although the cyclic turbulence spectra are similar at high frequency, the turbulence spectrum $\mathcal{S}_{ww,0}$,

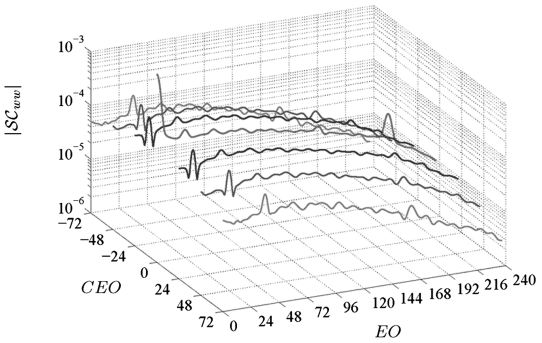

Fig. 7 Cyclic power spectrum applied to the measured velocity fluctuations.

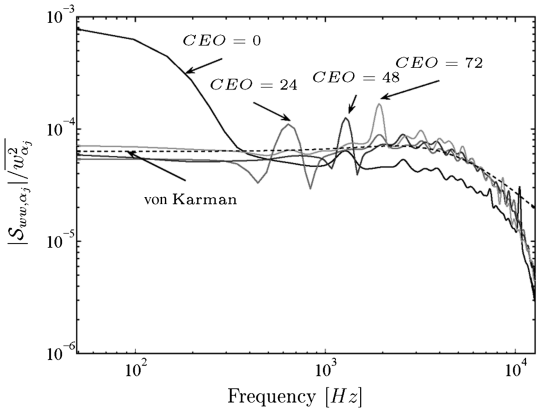

Fig. 8 Cyclic power spectrum for various values of CEO: 0, 24, 48, and 72, von Kármán model.

normalized by $\overline{w^2_{\alpha_0}}$, does not collapse with the normalized cyclic spectra for $\alpha_j \neq 0$. As shown in Fig. 6, $\overline{w^2_{\alpha_0}}$ is the sum of the background and nonperiodic wake components. It can be shown (not plotted here) that by normalizing $\mathcal{S}_{ww,0}$ by the value of $\overline{w^2_{\alpha_0}}$, due only to the wake, in Fig. 6, the spectra of Fig. 8 now collapse more closely, except at low frequencies.

An important quantity for characterizing the turbulence is the length scale Λ. For a stationary process, the turbulence length scale of the velocity component $w(t)$ is defined from the autocorrelation function $\mathcal{R}_{ww}(\tau)$, for example, by Pope [19], as

$$\Lambda = W \int \frac{\mathcal{R}_{ww}(\tau)}{\mathcal{R}_{ww}(0)}\, \mathrm{d}\tau \tag{24}$$

The aforementioned techniques have allowed the wake turbulence to be isolated from the background turbulence by performing spectral analysis in the cyclic frequency domain. To determine the length scale associated with the turbulent wake, Eq. (24) should be modified to include the cyclic autocorrelation function $\mathcal{R}_{ww,\alpha_j}$. The function $\mathcal{R}_{ww,\alpha_j}$ is often a complex function and a definition of the length scale by an analogous expression to Eq. (24) is not straightforward. An additional problem is that the cyclic autocorrelation function in Fig. 9 has strong oscillations due to presence of tones. The use of a modification to Eq. (24) for computing the length scale is therefore not meaningful in this application.

Figure 9 depicts the normalized cyclic autocorrelation functions $\mathcal{R}_{ww,\alpha_j}$ for various values of CEO. For CEO $\neq 0$, the cyclic autocorrelation functions collapse reasonably well in the vicinity of $\tau = 0$. Oscillations away from $\tau = 0$ are due to the peaks in the spectral coherence mentioned previously. Note that, for CEO $= 0$, the correlation decays very slowly to zero away from $\tau = 0$ due to the presence of very-low-frequency noise contamination, as observed in Fig. 8.

For a stationary process, an estimate of the length scale can be also obtained from the value of τ, at which the autocorrelation function $\mathcal{R}_{ww}(\tau)$ reaches half its maximum value of $\mathcal{R}_{ww}(0)$, as shown in Fig. 9, which gives a length scale equal to 1.35 mm.

Another common method for estimating Λ is through the low-frequency limiting behavior of the turbulence velocity frequency spectrum (see, for example, Ganz et al. [3]). The same principle can be applied to the spectrum at CEO $= 0$, such that

$$\Lambda = \frac{W}{2\overline{w^2_{\alpha_{j=0}}}} \lim_{f \to 0} \mathcal{S}_{ww,\alpha_{j=0}}(f) \tag{25}$$

where W is the mean velocity onto the stator. For the midspan measurement under investigation here, $W = 41$ m/s. However, because it has been shown in Fig. 8 that $\mathcal{S}_{ww,\alpha_j}/\overline{w^2_{\alpha_j}}$ is very similar for $\alpha_j \neq 0$, Eq. (25) predicts a similar turbulence length scale of $\Lambda_w = 1.5$ mm for each CEO, suggesting that Λ does not evolve through the wake. Devenport et al. [20] have measured the velocity spectra through the plane wake generated by a fixed profile. A very similar shape of the velocity spectra through the wake can be also observed. Note that the two estimates of the turbulence length scale are consistent.

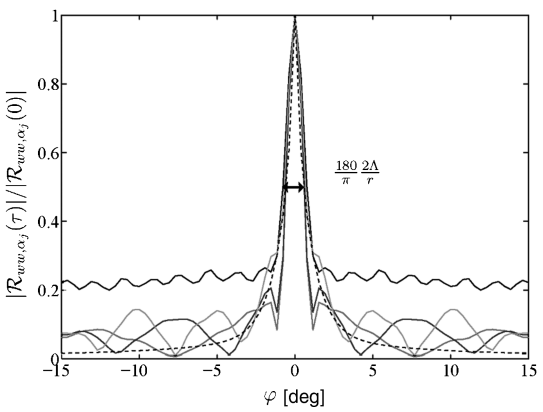

Fig. 9 Normalized cyclic autocorrelation function for various values of CEO: 0, 24, 48, and 72, von Kármán model. (The dashed line represents the autocorrelation modeled by von Kármán.)

3. *Background Turbulence Characteristics*

In the preceding section, the wake turbulence has been isolated from the background turbulence by using cyclostationarity analysis applied in the cyclic frequency domains, (α, f) or (α, τ). Similarly, the representations in the time domains (t, f) and (t, τ) will allow the determination of the background characteristics independently of the wake turbulence characteristics.

The background turbulence frequency spectrum can therefore also be deduced separately from the wake turbulence spectrum by the use of the Wigner–Ville spectrum applied to the fluctuating velocity component. The Wigner–Ville spectrum $\mathcal{WV}_{ww}$ is an estimate of the time evolution of the frequency spectrum and is plotted in Fig. 10 versus frequency and circumferential blade position, over four blade passages. In Fig. 10, the Wigner–Ville spectrum has been estimated by assuming a cycle duration of $T = t_{\mathrm{rot}}$ to allow the blade-to-blade differences on the time evolution of the spectra to be observed. The background turbulence power spectrum in the Wigner–Ville spectrum of Fig. 10 can be observed to have a completely different character to that of the wakes. The peaks observed in the cyclic power spectra at half the BPF and its harmonics are clearly identifiable and occasionally take negative values due to interaction terms in the estimation of the Wigner–Ville spectrum as discussed, for example, by White and Hammond [21].

Figure 11a shows a slice through the Wigner–Ville spectrum of Fig. 10 for various blade positions in between the wakes corresponding to the background turbulence. Figure 11b is a plot of the modulus of the same data plotted on a logarithmic scale.

In between the wakes, the turbulence spectra above 800 Hz, plotted in Fig. 11, oscillate about zero. Negative spectral components are nonphysical and are an artifact of the cyclostationarity technique. The validity of the spectral estimate in between the wakes is therefore highly questionable. Estimates of the turbulence length scale from these data give unrealistically large results.

4. *Instantaneous Autocorrelation Function*

The instantaneous autocorrelation function $\mathcal{R}_{ww}(t, \tau)$, obtained by the inverse Fourier transform of the Wigner–Ville spectrum with respect to f, is plotted in Fig. 12 for four adjacent blades. The autocorrelation function, as expected, exhibits small differences between adjacent wakes. The wakes are characterized by high correlation levels, whereas, in between the wakes, where only the background turbulence is present, the correlation is much smaller and more uniformly distributed across τ. Note that, for zero lag angle $(\varphi = 0)$, $\mathcal{R}_{ww}(t, 0)$ corresponds to the instantaneous variance plotted previously in Fig. 5.

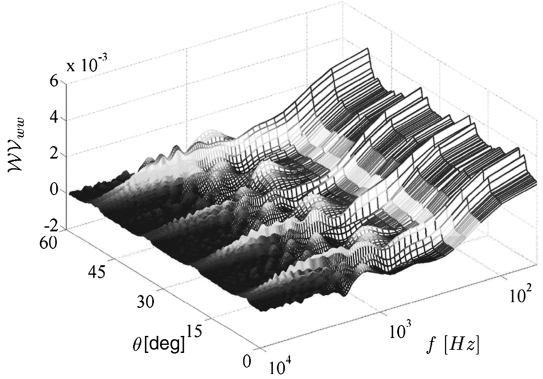

Fig. 10 Wigner–Ville spectrum applied to the measured velocity fluctuations.

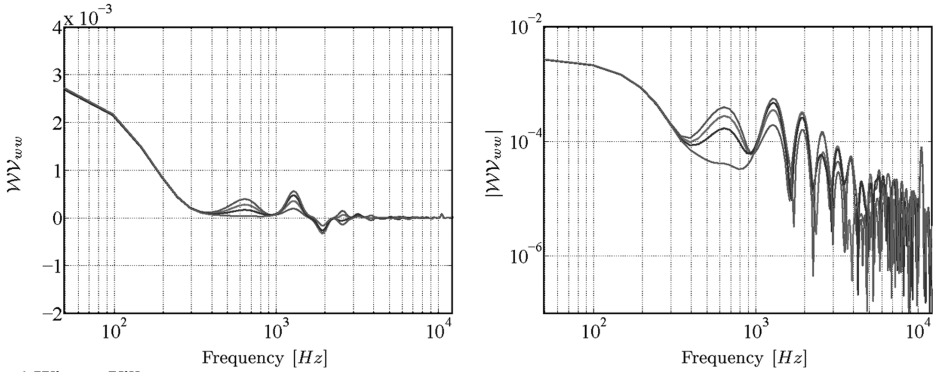

a) Wigner-Ville spectrum **b) Absolute value of Wigner-Ville spectrum**

Fig. 11 Wigner–Ville spectrum for various pitch angles at 6.9, 7.3, 7.7, and 8 deg.

The width of the peaks in this figure are determined by two length scales: the wake width L_w and the integral length scale Λ, and can be represented in a contour plot of the instantaneous autocorrelation function, normalized by its maximum, as shown in Fig. 13. In this paper, the wake width L_w is defined as the distance between the points at which the rms velocity deficit is 50% of its maximum value on the wake centerline, as proposed by Ganz et al. [3]. This figure suggests that, in this example, the two length scales are related by $\Lambda/L_w = 21\%$. This finding is in close agreement with the ratio measured by Ganz et al. [3].

Figure 12 is plotted again versus φ in Fig. 14a for three positions in the first wake. The three curves collapse extremely well, confirming, once again, that the wake turbulence statistics are invariant to position through the wake. Figure 14b shows the instantaneous autocorrelation function evaluated at the wake centerline for three different wakes. Again, the curves collapse, suggesting that the different blade wakes are very similar.

V. Model of the Wake and Background Turbulence

In this section, we seek to derive a simple expression for the space–time characteristics of the turbulence generated by the rotor. It must have all the characteristics identified by the cyclostationary and Wigner–Ville analysis presented earlier. The main finding of this analysis is that the wake turbulence characteristics, such as instantaneous variance (Fig. 5), length scale, instantaneous spectra (Fig. 8), and correlation function (Fig. 9) are essentially invariant to position through the wake. These quantities are simply modulated by the wake profile, which may be closely approximated by a simple Gaussian function. Following the results of Fig. 10, the Wigner–Ville spectrum $\Phi_{ww}(t, f)$, for example, may be written as the product of a spectrum $\Phi_{ww}(f)$ that has the properties of isotropic homogeneous turbulence and a periodic train of wake profiles. Thus, the spectral density of the rotor turbulence velocity at any point downstream of the rotor may be expressed in the form

$$\Phi_{ww}(t,f) = \overline{w_b^2}\Phi_b(f) + \overline{w_w^2}\Phi_w(f)\sum_{n=-\infty}^{\infty}\exp\left[-4\,\ell_n 2\left(\frac{r\Omega(t-nT_{\mathrm{BPF}})}{L_w}\right)^2\right] \tag{26}$$

where Φ_b and Φ_w are, respectively, the normalized background and wake power spectral densities and are time independent.

Figure 8 suggests that Φ_b and Φ_w follow very closely that for a von Kármán spectrum for homogeneous isotropic turbulence of the form

$$\Phi_{ww}(f) = \frac{2\Lambda}{3W}\frac{(3+8\pi A^2)}{(1+\pi A^2)^{11/6}} \qquad \text{with} \quad A = \frac{2\Gamma(1/3)}{\Gamma(5/6)}\frac{f\Lambda}{W} \tag{27}$$

Integrating Eq. (26) over f yields the instantaneous variance variation with t, observed in Figs. 5:

$$\overline{w^2}(t) = \overline{w_b^2} + \overline{w_w^2}\sum_{n=-\infty}^{\infty}\exp\left[-4\,\ell_n 2\left(\frac{r\Omega(t-nT_{\mathrm{BPF}})}{L_w}\right)^2\right] \tag{28}$$

Taking the Fourier transform of Eq. (26) with respect to t yields an expression for the cyclostationary spectral measurements of Fig. 7:

$$\mathcal{SC}_{ww}(\alpha,f) = \overline{w_b^2}\Phi_b(f)\delta(\alpha) + \overline{w_w^2}\Phi_w(f)\frac{L_w}{2r\Omega}\sqrt{\frac{\pi}{2\,\ell_n 2}}\exp\left[-\frac{1}{\ell_n 2}\left(\frac{\pi L_w\alpha}{2r\Omega}\right)^2\right]\frac{1}{T}\sum_{j=-\infty}^{\infty}\delta\left(\alpha+\frac{j}{T}\right) \tag{29}$$

Finally, integrating this expression over f yields the variation of turbulence energy with α plotted in Fig. 6:

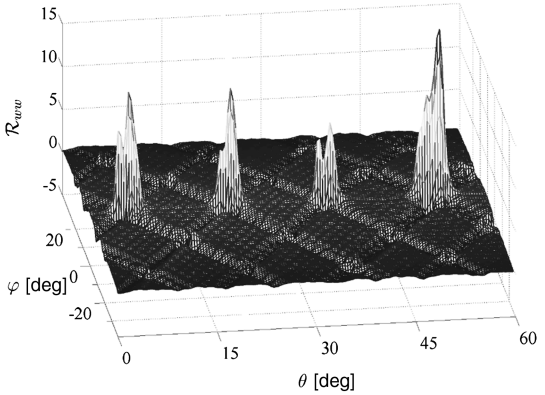

Fig. 12 Instantaneous autocorrelation function applied to the measured velocity fluctuations.

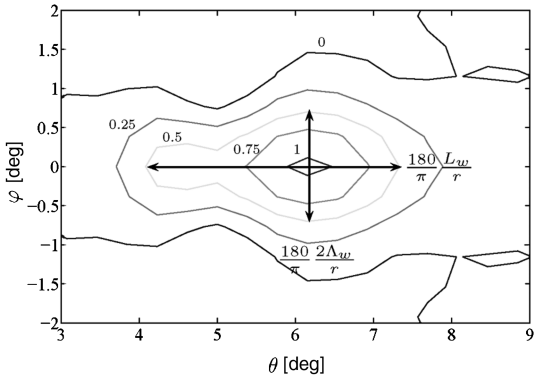

Fig. 13 Contour plot of the normalized instantaneous autocorrelation function.

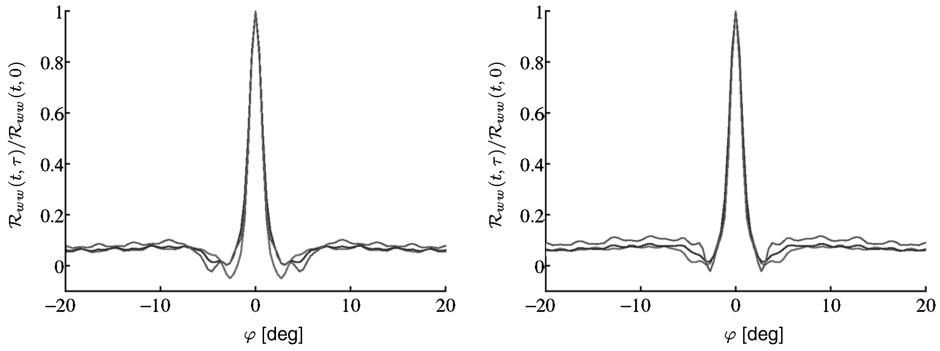

a) Same wake **b) Various wake centerline positions**

Fig. 14 Normalized instantaneous autocorrelation function for various time positions around the centerline of a) the same wake and b) for various wakes at the centerline.

$$\overline{w_{\alpha_j}^2} = \overline{w_b^2}\delta(\alpha) + \overline{w_w^2}\frac{L_w}{2r\Omega}\sqrt{\frac{\pi}{\ell_n 2}}\exp\left[-\frac{1}{\ell_n 2}\left(\frac{\pi L_w \alpha}{2r\Omega}\right)^2\right]\frac{1}{T}\sum_{j=-\infty}^{\infty}\delta\left(\alpha+\frac{j}{T}\right) \tag{30}$$

Note that $\overline{w_{\alpha_j}^2}$, modeled by Eq. (30), corresponds to the values of the Gaussian plotted in Fig. 6 at the cyclic frequencies $\alpha_j = j/T_{\text{BPF}}$. The spectral correlation for α_j, with $j \neq 0$, nondimensionalized by $\overline{w_{\alpha_j}^2}$ of Eq. (30), corresponds to the von Kármán turbulence spectrum of Eq. (27) and plotted in Fig. 8.

VI. Conclusions

The cyclostationary analysis method has been applied for the first time to turbulent velocity data measured behind a rotor on a scale-model ducted fan rig. Conventional stationary spectral analysis has been introduced as a special case of cyclostationary analysis. It has been shown that the wakes from different blades are statistically identical. Cyclostationary spectral analysis via its various time-frequency representations has allowed the background and wake spectral characteristics to be separated. The wake turbulence has been described in detail. However, the estimation of the background turbulence spectrum has been found to be problematic, as the background turbulence intermingles with interference "junk" terms due to small remaining coherence in the fluctuating signals. A model of the upwash fluctuating velocity downstream a rotor has been also proposed in the form of a simple homogeneous isotropic turbulence model, modulated by a Gaussian function.

Acknowledgments

This study has been carried out within the European-funded project PROBAND. The authors are grateful to Paul White for suggesting cyclostationary analysis to this problem. The authors are also grateful to Antoine Moreau, Lars Enghardt of DLR-Berlin, and Hans Boden of Kungliga Tekniska högskolan for providing the velocity data.

References

[1] Nallasamy, M., and Envia, E., "Computation of Rotor Wake Turbulence Noise," *Journal of Sound and Vibration*, Vol. 282, Nos. 3–5, 2005, pp. 649–678. doi:10.1016/j.jsv.2004.03.062

[2] Jurdic, V., Moreau, A., Joseph, P., Enghardt, L., and Coupland, J., "A Comparison Between Measured and Predicted Fan Broadband Noise Due to Rotor-Stator Interaction," AIAA 2007-3692, 2007.

[3] Ganz, U. W., Joppa, P. D., Patten, T. J., and Scharpf, D. F., "Boeing 18-Inch Fan Rig Broadband Noise Test," NASA CR-1998-208704, 1999.

[4] Gliebe, P., Mani, R., Shin, H., Mitchell, B., Ashford, G., Salamah, S., and Connell, S., "Aeroacoustic Prediction Codes," NASA CR-2000-210244, 2000.

[5] Antoni, J., Bonnardot, F., Raad, A., and El Badaoui, M., "Cyclostationary Modelling of Rotating Machine Vibration Signals," *Mechanical Systems and Signal Processing*, Vol. 18, No. 6, 2004, pp. 1285–1314. doi:10.1016/S0888-3270(03)00088-8

[6] Bonnardot, F., Randall, R. B., and Guillet, F., "Extraction of Second-Order Cyclostationary Sources: Application to Vibration Analysis," *Mechanical Systems and Signal Processing*, Vol. 19, No. 6, 2005, pp. 1230–1244. doi:10.1016/j.ymssp.2005.07.008

[7] Tardu, S., *Caracterisation des ecoulements turbulents instationnaires periodiques*, Éditions Scientifiques et Médicales Elsevier, Paris, 2003.

[8] Hardin, J. C., and Miamee, A. G., "Correlation Autoregressive Processes with Application to Helicopter Noise," *Journal of Sound and Vibration*, Vol. 142, 1990, p. 2.

[9] Gardner, W. A., Napolitano, A., and Paura, L., "Cyclostationarity: Half a Century of Research," *Signal Processing*, Vol. 86, No. 4, 2006, pp. 639–697. doi:10.1016/j.sigpro.2005.06.016

[10] Boyles, R. A., and Gardner, W. A., "Cycloergodic Properties of Discrete-Parameter Nonstationary Stochastic Processes," *IEEE Transactions on Information Theory*, Vol. 29, Jan. 1983, pp. 105–114. doi:10.1109/TIT.1983.1056613

[11] Braun, S., "The Extraction of Periodic Waveforms by Time Domain Averaging," *Acustica*, Vol. 32, No. 2, 1975, pp. 69–77.

[12] Gardner, W. A., *Statistical Spectral Analysis: A Nonprobabilitic Theory*, Prentice–Hall, Upper Saddle River, NJ,1987.

[13] Evans, R. L., "Turbulence and Unsteadiness Measurements Downstream of a Moving Blade Row," *Journal of Engineering for Power*, Jan. 1975, pp. 131–139.

[14] Martin, W., and Flandrin, P., "Wigner–Ville Spectral Analysis of Nonstationary Processes," *IEEE Transactions on Acoustics, Speech, and Signal Processing*, Vol. 33, No. 6, 1985, pp. 1461–1470. doi:10.1109/TASSP.1985.1164760

[15] Moreau, A., Enghardt, L., and Boden, H., "On the Relation Between Broadband Noise and Aerodynamic Fan Performance," Inst. of Noise Control Engineering–Europe, Paris, 2007.

[16] Amiet, R. K., "Acoustic Radiation from an Airfoil in a Turbulent Stream," *Journal of Sound and Vibration*, Vol. 41, No. 4, 1975, pp. 407–420. doi:10.1016/S0022-460X(75)80105-2

[17] Wygnanski, I., Champagne, F. H., and Marasli, B., "On the Large-Scale Structures in Two-Dimensional, Small-Deficit, Turbulent Wakes," *Journal of Fluid Mechanics*, Vol. 168, No. 1, 1986, pp. 31–71. doi:10.1017/S0022112086000289

[18] Antoni, J., "Cyclic Spectral Analysis in Practice," *Mechanical Systems and Signal Processing*, Vol. 21, No. 2, 2007, pp. 597–630. doi:10.1016/j.ymssp.2006.08.007

[19] Pope, S. B., *Turbulent Flows*, Cambridge Univ. Press, Cambridge, England, U.K., 2000.

[20] Devenport, W. J., Muthanna, C., Ma, R., and Glegg, S. A., "Measurement and Modeling of the Two-Point Correlation Tensor in a Plane Wake for Broadband Noise Prediction," NASA Rept. VPI-AOE-263, May 1999.

[21] White, P. R., and Hammond, J. K., "Signal Processing Techniques," *Advanced Applications in Acoustics, Noise and Vibration*, Spon Press, London, 2004.

S. Fu
Associate Editor